

# Interactive Segmentation of Radiance Fields

Rahul Goel

Dhawal Sirikonda

Saurabh Saini

PJ Narayanan

CVIT, IIT Hyderabad

{rahul.goel, dhawal.sirikonda, saurabh.saini}@research.iit.ac.in, pjn@iit.ac.in

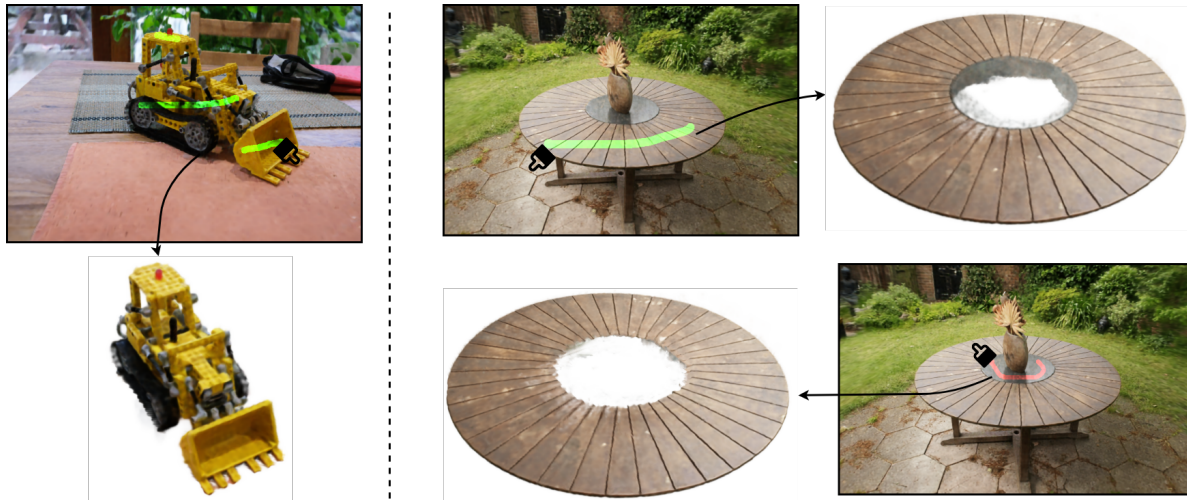


Figure 1. We present an interactive method to segment objects in radiance fields. Like GrabCut, users draw strokes to segment multiple objects at a time in 3D. Users can indicate negative strokes to remove unwanted regions if they appear. Left: Segmented JCB. Right: Segmented table-top with positive and negative strokes

## Abstract

*Radiance Fields (RF) are popular to represent casually-captured scenes for new view generation and have been used for applications beyond it. Understanding and manipulating scenes represented as RFs have to naturally follow to facilitate mixed reality on personal spaces. Semantic segmentation of objects in the 3D scene is an important step for that. Prior segmentation efforts using feature distillation show promise but don't scale to complex objects with diverse appearance. We present a framework to interactively segment objects with fine structure. Nearest neighbor feature matching identifies high-confidence regions of the objects using distilled features. Bilateral filtering in a joint spatio-semantic space grows the region to recover accurate segmentation. We show state-of-the-art results of segmenting objects from RFs and compositing them to another scene, changing appearance, etc., moving closer to rich scene manipulation and understanding. [Project Page](#)*

## 1. Introduction

Scene representation is a crucial step prior to any scene understanding or manipulation task. Relevant scene parameters, be it shape, appearance or illumination, can be represented using a variety of modalities like 2D (depth/texture) maps, point clouds, surface meshes, voxels, parametric functions *etc.* Each modality facilitates some task while taxing some other aspect of the process. For example, shape correspondence is straightforward between point clouds compared to surface meshes but compromises on rendering fidelity. Thus, choosing an appropriate representation has a major impact on the downstream analyses and applications.

Neural implicit representations have emerged as most promising modality for 3D analysis recently. Although initially proposed only for shapes [27, 33], such representation have been extended to encode complete directional radiance at a point [29] and to other rendering parameters like lightfields, specularities, textual context, object semantics, *etc.* [1, 9, 11, 12, 15, 18, 48]. These representations are

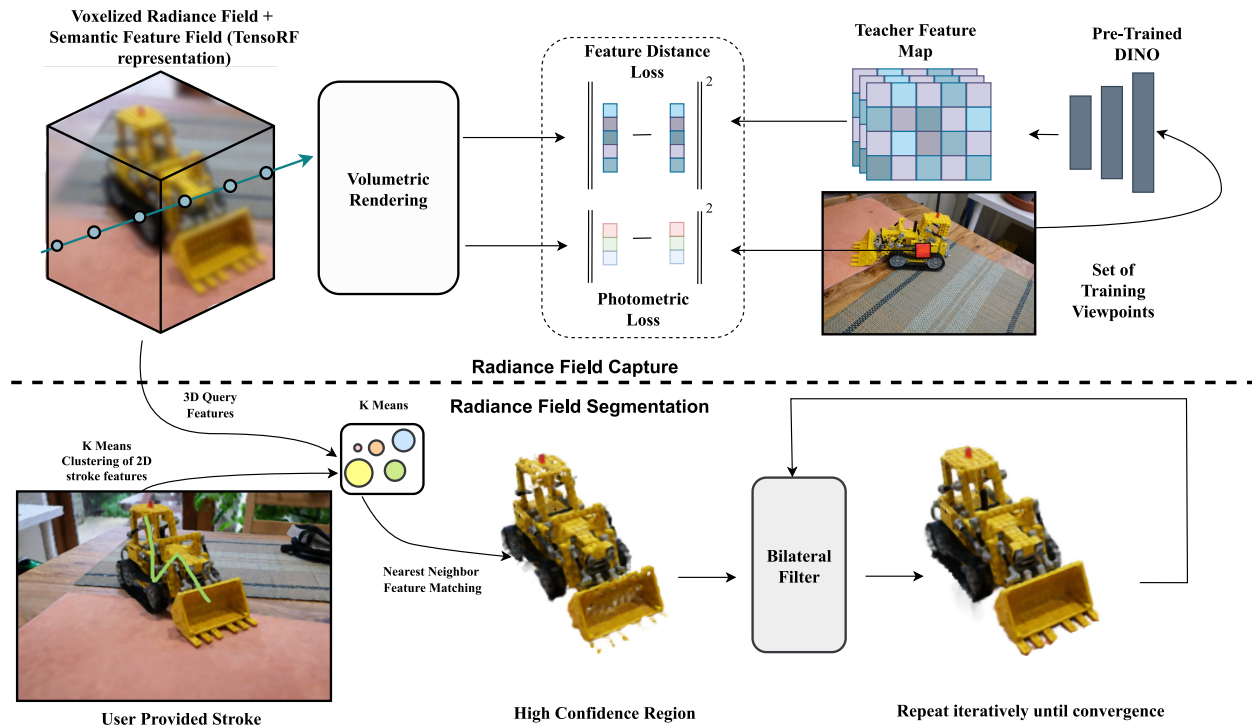


Figure 2. *System overview*: We capture a 3D scene of voxelized radiance field and distill the semantic feature into it. Once captured, the user can easily mark a regions using a brush tool on a reference view (green stroke). The features are collected corresponding to the marked pixels and clustered using K-Means. The voxel-grid is then matched using NNFM (nearest neighbor feature matching) to obtain a high confidence seed using a common tight threshold. The seed is then grown using bilateral filtering to smoothly cover the boundaries of the object, conditioning the growth in the spatio-semantic domain.

being extended beyond the simpler static inward-looking and front-facing scenes to complex outwards-looking unbounded  $360^\circ$  views, dynamic clips, heavily occluded ego-centric videos and unconstrained *wild* images.

Radiance fields have also been used beyond Novel View Synthesis (NVS) for other applications [5, 25, 34, 42, 44, 46, 50, 53, 56]. MLP-encoded representations like NeRF cannot be manipulated easily. Segmenting objects of the scene representation is a first step towards its manipulation and understanding for different downstream tasks. There have been a few efforts at segmenting and editing of radiance fields. Recently, N3F [45] and DFF [20] have proposed preliminary solutions to this in the neural space for the radiance field representation. Both use distillation for feature matching between user provided cues with the learned 3D feature volume, with N3F using user-provided patches and DFF using textual prompts or patches as the segmentation cues. These methods struggle to segment objects that have wide variation in its appearance.

In this paper, we present a simple and efficient method to segment objects in a radiance field representation. Our segmentation as an intuitive process with the user providing easy strokes to guide it interactively. We use the TensorRF

representation [7] which is both memory-efficient and fast to train and render. TensorRF uses an explicit voxel representation that is more amenable to manipulation. Our radiance field includes a DINO feature [6] at every voxel to facilitate semantic matching from 2D to 3D. We condense the DINO features from the user-specified regions to create a fixed-length set using K-Means. A tight, nearest neighbour feature matching (NNFM) of this set to features in the 3D voxels identifies a high-confidence seed region of the object to be segmented. The seed region is grown using bilateral filtering to include neighboring voxels that are proximate in a joint feature-geometry space. We show results of segmenting several challenging objects in forward facing [28] and 360 degree [2] scenes. The explicit voxel space we use facilitates simple modification of the segmented objects. We also show examples of compositing objects from one RF into another. In summary, following are our core contributions:

- An easily interpretable and qualitatively improved 3D object segmentation framework for radiance fields.
- Interactive modification of segmentation to capture fine structure, starting with high-confidence matching.

Our representation allows spatio-semantic bilateral filtering to make this possible.

- A hybrid implicit-explicit representation that is memory-efficient and fast to render that also facilitates the distillation of semantic information for improved segmentation. Our results show improved accuracy and fine-grain object details on very challenging situations over contemporary efforts.
- Segmentation comparisons on multiple scene types and usage on several downstream applications like NVS, appearance alteration, object replacement, *etc.*

## 2. Related Work

Radiance field research work is extensive and fast-growing. Hence, we restrict our related works discussion to three relevant topics *i.e.* hybrid representations, feature encoded extensions beyond shape and appearance and scene manipulation solutions in radiance fields. For a more comprehensive background, we encourage the reader to refer to the latest surveys in this area [43, 51].

**Hybrid Representations:** In the past several years, various representations have been employed for the NVS application [14, 22, 47]. The latest line of works based on implicit volumetric representations [2, 29, 29] specifically has shown great promise by leveraging the radiance fields for comprehensive scene representation. NVS from the perspective of radiance fields just involves image volumetric ray-traced rendering [29] from a particular viewpoint. But despite its vast utility, NeRF demands tens of hours of training time per scene. Computational overhead issue has been the focus of subsequent works like PlenOctrees [54], KiloNeRF [36] *etc.* which borrow efficient techniques from the traditional 3D literature. Later, Plenoxels [10] and DVGO [40, 41] have advanced more on this front by harnessing the lattice structure in a hybrid representation with implicit field features encoded on an explicit spatial grid. This significantly reduces the training time overhead to 5-10 minutes per scene by trading it off with an increase in storage requirement. InstantNGP [30] has even furthered the timing to a matter of seconds by the utilization of Multilevel hash encodings. Recently, TensorRF [7] has proposed a tensor decomposed a set of matrix-vector representation for the radiance feature lattice structure which addresses both the storage and time overhead issues. We base our method on TensorRF representation to take advantage of this gained efficiency and explicit geometric information.

**Editing:** The advent of NeRFs has paved a principled way for altering the appearance of 3D scene content. A plethora of works have followed up this approach for solving problems in varied domains on the editing problem. More specifically, works like [3, 4, 31, 39, 58] have disentan-

gled the photo-realistic rendering equation to account for the material and lighting edits. Whereas, others like [32] and [17, 55] have aimed to alter the appearance via post-hoc image-based stylization modules [13, 19]. Apart from such appearance edits, methods like [8], [52], have concentrated on geometric deformations of object-centric scenes represented as Radiance Fields. Our proposed method allows both appearance and geometric scene manipulations.

**Semantics:** For scene understanding the semantic information of the scene is essential still only a handful of solutions have been proposed in this area. Initial methods like Semantic NeRF [59] have tried to directly regress semantic labels in the novel views from sparse priors. While a few leverage the deep image features like DINO [6] and LSeg [23], to attribute semantics to the 3D scene points. N3F [45] and DFF [20] are two main works in this direction. Object-specific segmentation is possible in both of these methods since the deep semantics are 3D transferred and matched with the respective 2D counterparts. Though these methods support segmentation, interactive content addition and removal is not supported by these approaches as the underlying scene representation is an implicit neural function which prohibits easy alterations and easy extension into other application scenarios.

In this work, we use a similar 2D-3D distillation based approach like N3F and DFF but with a focus on fine-grained interactive segmentation. Initial works like GrabCut [37] and its variants have utilized positive and negative user strokes to obtain the correct segmented objects. Subsequent variants [24, 38] have augmented this by leveraging the deep learning both in the temporal and non-temporal domains. We draw inspiration from them and build upon on the proven traditional image, NN and voxel carving techniques [16, 21] by extending them to the domain of radiance fields. We experimentally prove how such simple techniques combined with the appropriate scene representation can improve result quality and fine details while simultaneously being quite intuitive, interpretable and efficient.

## 3. Method

We provide the basics on radiance fields and the feature distillation strategy related to our scene representation learning. We then detail our proposed interactive segmentation workflow comprising of 2D-3D feature matching, region growing and manipulation techniques on this learned representation.

### 3.1. Radiance Field Representation

A radiance field [60]  $\mathcal{F}$  maps the scene radiance values as view dependent RGB color  $c \in \mathbb{R}^3$ , given a continuous point  $x \in \mathbb{R}^3$  and viewing direction  $d \in \mathbb{S}^2$  in space as inputs:  $\mathcal{F}(x, d) : \mathbb{R}^3 \times \mathbb{S}^2 \rightarrow \mathbb{R}^3$ . NeRF [29] and its variants

[2,26,57] encoded this mapping as the neural function using an MLP, with low memory footprint but high training and rendering overhead. They also store scalar point density  $\sigma \in \mathbb{R}$  which is used for differentiable volumetric rendering to train the network:

$$\hat{C}(r) = \left( \sum_{i=1}^K T_i \alpha_i c_i \right) \quad \text{where} \quad (1)$$

$$\alpha_i = 1 - e^{-\sigma_i \delta_i} \quad \text{and} \quad T_i = \prod_{j=1}^{i-1} (1 - \alpha_j). \quad (2)$$

Here for a given point  $i$  along a ray,  $\delta_i$  is the distance to the sampled point,  $T_i$  is the accumulated transmittance, and  $c_i$  is the view-dependent color for the point. Later efforts like Plenoxels [10] and DVGO [40] stored the field variables in a lattice structure akin to 3D voxel grid, significantly improving the training and rendering times at the cost of high storage requirement. These quantized values are trilinearly interpolated and decoded to render color value at any point. The grid structure provides easy spatial context and explicit representation leads to higher efficiency. Recently, TensorRF [7] proposed a matrix-vector decomposition representation of this lattice that reduced that storage requirements while facilitating efficient training and view generation. We use TensorRF as the basis of our work. The top part of Fig 2 shows our radiance field capture step, with the volume represented using TensorRF. In the case of the quantized representation of radiance fields, the radiance is obtained as follows:

$$\sigma_i = \psi(V^\sigma, x_i) \quad \text{and} \quad c_i = \mu_\theta^{rgb}(\psi(V^f, x_i), d). \quad (3)$$

Here  $\sigma$  is the density of the volumetric space,  $V^f$  the radiance feature grid of appearance features  $f$ , and  $\psi$  indicates trilinear interpolation. While rendering a given sample point  $x_i \in \mathbb{R}^3$  along the ray direction  $d$ , a small decoding MLP  $\mu_\theta^{rgb}(f_i, d) \rightarrow c_i$  is evaluated. The final color of a ray is calculated by combining all sample colors  $c_i$  at every point  $x_i$  along it using the Eq 1. This is used to reduce the photometric loss  $\mathcal{L}^{(rgb)}$  optimizing for the both radiance feature lattice  $V^f$  and parameters  $\theta$  of MLP ( $\mu$ ).

### 3.2. Semantic Features Distillation

Object segmentation requires knowledge scene semantics. We include an additional feature into the radiance field for this. In order to attribute semantics to the radiance field, we distill contextual knowledge from a large pretrained teacher model similar to the prior art [20,45]. Specifically, our teacher is a vision transformer model trained using self-supervision and is shown to pay attention to semantically meaningful objects in the scene in a class agnostic manner. This knowledge from the teacher is distilled into the student radiance field in addition to the color and density values as point semantic features  $\phi \in \mathbb{R}^m$ . Thus the mapping now becomes:  $\mathcal{F}(x, d) : \mathbb{R}^3 \times \mathbb{S}^2 \rightarrow \mathbb{R}^3 \times \mathbb{R} \times \mathbb{R}^m$ . More concretely,

we use 2D semantic features using DINO ViT-b8 model [6] for each input posed image. Recent efforts [20,45] also use DINO; unlike them, we directly optimize for the features on the voxel grid in the TensorRF representation without a neural network. We also do not encode the direction dependence in these semantic features since the object semantics are direction agnostic. We evaluate trilinearly interpolate the distilled semantic feature  $\phi_i = \psi(V^\phi, x_i)$  for a point  $x_i$  from the learned feature lattice  $V^\phi$ . We combine the  $\phi_i$  along the ray using the Eq 1 like color  $c_i$ . The TensorRF representation is optimized to minimize the total loss

$$\mathcal{L} = \mathcal{L}_{rgb} + \lambda \mathcal{L}_{feature} \quad (4)$$

to obtain the final radiance field with  $\phi$ ,  $V^f$ , and  $V^\phi$ . Both losses  $\mathcal{L}_{rgb}$  and  $\mathcal{L}_{feature}$  are calculated using  $L^2$  norm.

High resolution feature rendering results in high-frequency feature fields similar to N3F [45]. (See the supplementary file for feature field visualizations.) Explicit semantic features at every point open the way to adapt traditional 3D analysis techniques in a semantically meaningful fashion to radiance fields. Segmenting objects in 3D voxel space and the use of bilateral filtering are examples, which go beyond what prior neural representations showed.

### 3.3. 2D-3D Feature Matching

For object segmentation, the user picks a reference view and annotates the regions of interest using a brush stroke. Semantic DINO features associated with the marked pixels are collected. DINO features were shown to fare well using 1-NN feature matching for good 2D semantic segmentation [6]. However, a single DINO feature will not suffice to segment complex objects with diversity. We cluster the input features using K-Means to obtain a fixed-size exemplar set of features for matching in 3D space. We use nearest neighbor feature matching (NNFM) on the exemplar set to label each voxel as foreground or background. The result is stored in a 3D bit-map. We use a tight threshold in this step to identify a seed region of high-confidence, which are processed further. Prior methods [20,45] used a single averaged semantic feature from the user-specified patch to match 2D to 3D. Their implicit neural representation can only perform segmentation after  $\phi$  values are rendered. Feature matching methods like NNFM are too costly to evaluate at every point on the ray using a neural representation. The segmentation results can also be precomputed and stored, facilitating downstream tasks like view generation and editing on the fly, without repeated processing.

### 3.4. Region Growing

The high confidence seed region ( $M^0$ ) from the previous step is grown in the volume-space to delineate the complete object volume. We do this in a joint spatio-semantic

space to include proximate voxels that are also close semantically. We adapt a *Bilateral Filtering* method on the voxel grid using the spatial feature  $x$  and semantic feature  $\phi$  values as filter’s domain and range kernels respectively. We iteratively grow the current bitmap region  $M^r$  till convergence as given below.

$$M^{r+1}(x) = \mathcal{T}_\tau \left( \frac{1}{W} \sum_{x_i \in \Omega_x} M^r(x_i) g_{\sigma_\phi}(\phi_i^2) g_{\sigma_s}(s_i^2) \right)$$

where  $\phi_i = \|\phi_{x_i} - \phi_x\|$ ,  $s_i = \|x_i - x\|$   
and  $W = \sum_{x_i \in \Omega_x} g_{\sigma_f}(\phi_i^2) g_{\sigma_s}(s_i^2)$ .

Here  $M^r$  is the  $r^{th}$  iteration of filtering;  $\phi_x$  is the distilled semantic feature at point  $x$  in the volumetric space;  $g_\sigma$  is the Gaussian smoothing functions with variance  $\sigma$ ;  $\mathcal{T}_\tau$  is binary thresholding against value  $\tau$ ; and  $\Omega_x$  is the immediate voxel neighbors of  $x$ . We find that  $\tau = 0.2$  works well for our scenes. The seed region expands to the boundaries of the desired object in a few iterations of bilateral filtering.

### 3.5. User Interactivity

Region growing results in a stable voxel content based on the input strokes. The user can add or remove parts interactively if the extracted content misses out on a few details or when some extraneous content floods into the segmented region. We use positive and negative strokes to add and remove content in the image space, as followed by methods like GrabCut [37]. The mask of negative segment is subtracted from the mask of the positive segment to get the final segmented objects. We find practically that even complex objects can be segmented well with a few positive and negative strokes as shown in results in the paper and in the supplementary material.

Due to space constraints, complete implementation details have been reported in the supplementary pdf.

## 4. Results

In this section, we discuss the comparisons and results of our proposed method against the existing semantic features distillation based Radiance fields segmentation approaches. Specifically, we focus on the two recent approaches (1) DFF-DINO [20] (Distilled Feature Fields using DINO as the backbone) and (2) N3F [45] (Neural Feature Fusion Fields). Both aforementioned methods make use of the extracted features from an input image set to fuse them into the volumetric space. DFF additionally concentrates on the language queries using LSeg [23], but both the approaches are similar in the case of semantic features. As the code of DFF is not publicly available, we compare our method against N3F, which is similar to DFF for this part.

### 4.1. Comparison

As discussed earlier, our approach supports region selection either by a patch or a hand-drawn brush stroke as shown in Fig.1. We follow the methods described in the Sections (3.3, 3.4) to obtain the desired volumetric content. The Fig.3 shows our segmentation results.

The usage of clustering followed by NNFM clearly outperforms the prior approach of average matching [20, 45]. The direct incorporation of nearest neighbor feature matching (NNFM) in these approaches leads to significant rendering delays, while the choice of neural space limits them from using elegant techniques like Bilateral filtering.

In Fig.3 it can be observed that in the case of the COLOR FOUNTAIN, the simple average feature matching technique faithfully recovers the region of interest albeit some additional noise. But as the complexity of the scene and region of interest grows, the prior art fails to garner pleasing results. This can be observed clearly in the case of the three LLFF [28] scenes (CHESS TABLE, SHOE RACK, STOVE). The CHESS TABLE scene suffers due to the erroneous feature matches when only simple averaging is employed. The clustered matching mitigates the errors and confines the segmented volume to the TABLE. A similar effect can be observed in the case of STOVE where the object of interest is sparingly covered in the input images but is faithfully recovered with distinct boundaries, unlike N3F. The last scene SHOE RACK is a classical example where even with the best feature matching scheme, recovering white-sole might be challenging. This is where the Bilateral filtering helps in exploiting multi-domain content exploration by conditioning on the spatio-semantic domain. A detailed depiction of these results are discussed in the supplementary.

### 4.2. Region Growing: Bilateral Filter

In this section, we discuss the effect of bilateral filtering on the radiance fields and how it improves the final result. Even after employing an efficient feature-matching technique, we often obtain a high-confidence volumetric region but with missing constituting parts. This is because that the content search is solely dependent on feature distances while completely ignoring the spatial priors. To resolve this issue we resort to Bilateral filtering which exploits spatio-semantic domain priors resulting in accurate segmentation constituting all the desired regions of the semantic object. This is demonstrated in Fig.4, where the initial high-confidence region misses the outer leaf of the dry plant. While bilateral region growing, we iteratively add more details into the extracted region finally obtaining desired volumetric content. This content can be further used for various purposes as discussed in Sec.5.2.



Figure 3. Results of N3F/DFF [20,45] against ours. Both N3F and DFF employ a similar strategy for segmentation. We tweak the threshold for their method and bring out the best results and show their respective results in the Row 2. Row 3 shows our results with the same queried patch (highlighted in green in Row 1). Since our method works best on user provided strokes, we show the corresponding results in Row 4. While N3F/DFF are able to recover simpler objects like COLOR FOUNTAIN, they fail to capture other objects. Our method faithfully recovers the queried objects with clear and smooth boundaries. For more details, please refer to Sec 3.4.



Figure 4. *Region Growing*: Image (a) is the reference rendered viewpoint. Image (b) is the high confidence region which misses out frontal region of the dry-leaf when extracting the content. Image (c) shows the result obtained after the first iteration of bilateral filtering, which captures most of the desired region of the leaf. Image (d) is the result of the bilateral filtering applied for the second time to include intricate details such as strands around the dry-leaf.

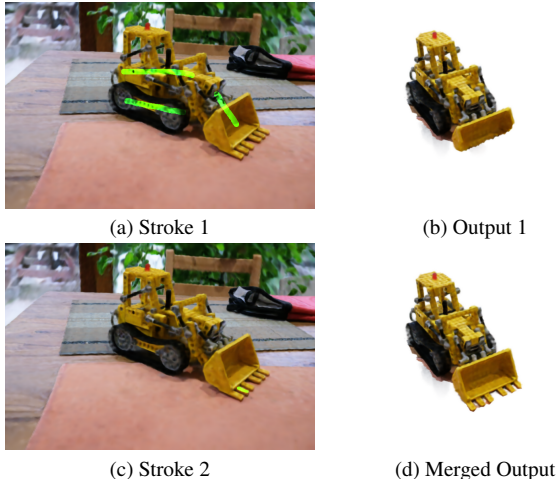


Figure 5. *Multiple Positive Strokes*: When the method fails to capture some of the details using one stroke, the user can add more positive strokes to recover the object of interest. Here, the user makes three strokes in (a). The teeth of the JCB are not extracted well in (b). When the user makes an additional stroke on one of the teeth (c) and the resultant image (d) capture the full details.

### 4.3. Interactive Segmentation: Positive and Negative Strokes

Our method allows both addition and removal of content using positive and negative strokes. The cases where the single stroke fails to obtain the desired content in the extracted space, the user can add another positive stroke to add more content. Fig.5 shows one such example where the excavator (‘JCB’) has missing teeth in the extracted region. By drawing an additional stroke and bilaterally growing the region again brings out the full desired result. This effectively grows the bit-map  $M^r$  by segmenting more desirable regions from the volumetric space.

Similar to addition of new content, some scenarios demand the need for the removal of extraneous content from the extracted region. In such scenarios, we mark the region to be removed and grow it independently of the positive content. Once fully grown, full extent of the negative/undesirable content is obtained which we subtract from the previously extracted regions obtaining the edited bit-map  $M^r$ . Fig.1 shows one such example where the REFLECTIVE GRANITE floods into the TABLE region. We add a negative stroke (red) to remove this undesired region.

The incorporation of these functionalities is not trivial in the case of the prior art, as an additional negative match or a positive match calculation at the time of rendering is a tedious task.

## 5. Experiments

In this section, we discuss our various feature matching variants which we used for obtaining the high-confidence seed region. Additionally, we show some immediate applications of radiance field segmentation.

### 5.1. Ablations

In order to obtain a high-confidence region, which acts as a seed for the bilateral filter, a feature-matching technique is required to match the marked features with the distilled semantic features in the volumetric space. To this end, we experimented with three different feature matching techniques namely (1) Average Feature Matching, (2) Nearest neighbor Feature matching(NNFM) (3) K means + NNFM, which are compared in the Fig.7. It can be easily inferred from Fig.7(b) that average feature matching performs very poorly in this task. In order to improve these results we resort to the nearest neighbor feature matching. Though this recovers a good high confidence region, it is accompanied by additional noise as seen in Fig.7(c). Furthermore, as the marked region’s size grows, computation also becomes tedious in this case. To can be addressed when we cluster the features using K-means clustering and then do an NNFM whereby reducing computational overhead and avoiding noisy matches as seen in Fig.7(d).

### 5.2. Editing

After obtaining a good segmentation, the next required task might be manipulation and re-rendering. We present four illustrative editing examples: (1) Object Removal, (2) Translation, (3) Appearance Editing and (4) Geometric Scene Composition.

**Object Removal:** The removal of an object from scene is a simple task and is shown in the Fig.6(a) where the POT in GARDEN scene is removed. To obtain this result we select a patch consisting of the POT in the reference image and follow the steps mentioned in Sec.3.4 to obtain the final bit-map of the pot  $M^r$ . With a simple flipping of the bit-map ( $M^r$ ), the background can be obtained ( $M^r$ ), which is then used to render the demonstrated results Fig.6(a). Please note that we did not inpaint the scene post content removal.

**Affine transformation:** As we have a good quality segmented volumetric content, we can perform affine transformations on voxel space (POT) for object position manipulation. We demonstrate this in Fig.6(b). One can look *behind* the TABLE on the GROUND to see the repositioned POT.

**Appearance Editing:** As we have the appearance vector associated with each voxel in the grid, we can alter the appearance of the individual segmented objects. Here we demonstrate it in Fig.6(c) by changing the color of the POT.

**Geometric Scene Composition:** We using high quality

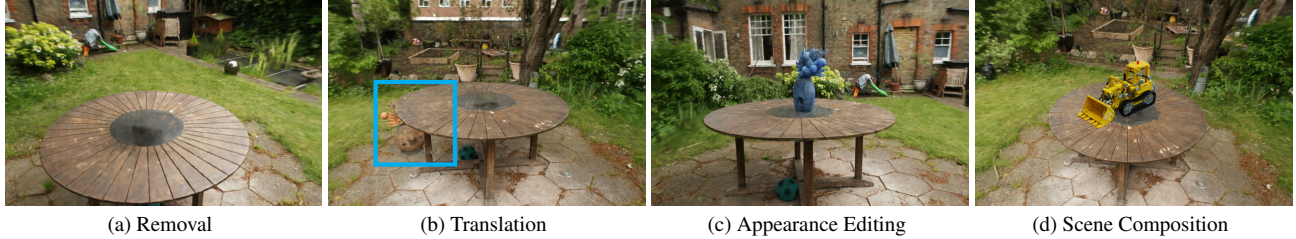


Figure 6. *Scene manipulation*: Once an object is segmented, we can edit it in different ways. This allows us to manipulate the underlying scene in multiple straightforward ways. In (a), we remove the POT from the center of the table. In (b), we translate the POT to the GROUND behind the TABLE. In (c), we change the appearance of the POT to bluish shade by simple changing RGB to BGR. More complex edits appear in the supplementary document. In (d), we replace the POT with the LEGO JCB obtained from a different scene (KITCHEN). The scenes are picked from [2].

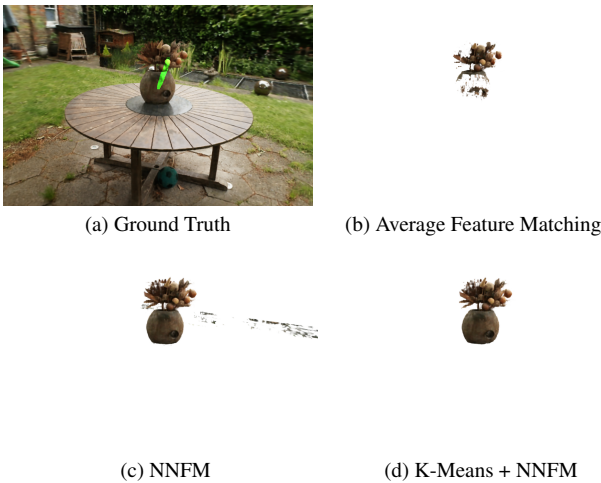


Figure 7. *Feature Matching*: In this figure, the high confidence region for image in (a) is obtained using different feature-matching algorithms for a particular stroke. (b) Average feature matching fails to cover the entire object due to loss of information during the averaging process. (c) Nearest Neighbor Feature Matching without clustering leads to noise bleeding. (d) NNFM after clustering eliminates noisy regions while matching multiple features at once.

object segments, we can also composite two radiance fields from different scenes. Please note that we only focus on geometric composition, and do not attempt correct global illuminations as such variables were never processed in the underlying representation. We demonstrate this in Fig.6(d). We follow the composition technique of [49] to accomplish this task. The JCB is picked from the KITCHEN scene from the [2] dataset and placed in GARDEN.

## 6. Discussions and Conclusions

In this paper, we presented an easy and accurate method to segment objects from a TensorRF representation of radiance fields and showed simple scene editing operations

facilitated by this. The efficient voxel-based representation we use makes our method more versatile and simple compared to the prior works in this direction. We show several results on multiple challenging scenes (and present more in the supplementary document). Semantic segmentation is a first step towards interpretation, understanding, and manipulation of 3D scenes. This work provides high quality segmentation that can be the basis for several such downstream tasks.

Our method improves upon the prior art on several fronts but has its own shortcomings. Like prior works, we rely on DINO features to represent object semantics and this can result in artefacts if the features do not capture the semantics properly. Third column in the last row in Fig 3 shows a small false appendage at the bottom of the utensil holder which can not be easily removed interactively without eating into object’s body. Better semantic features can resolve this problem. Also, the leftmost example in Fig 6 shows that the shadow of the pot is left behind on the granite center of the table even after the pot is edited out. Removing the pot from the geometric representation does not guarantee removal of its secondary effects on neighbouring objects like shadows or highlights, without elaborate geometric post-processing. Our method may also struggle in segmenting geometry well if the voxel resolution is low compared to the scale of object details as shown in supplementary results. Multiresolution voxel representations can solve this problem with additional overhead.

In the future, multi-representation processing might be needed by combining parts of captured RFs, graphics models, SDFs, etc., to provide maximum flexibility in Virtual Reality and Augmented Reality applications. This requires processing parts of the RFs directly without going through the full learning process post-editing. This is a promising direction of work that we intend to pursue in the future.



**Potential negative societal impacts:** Our work presents a tool to manipulate radiance fields captured casually. While ill-intentioned manipulation to create the appearance to fake scene content is possible using such a tool, the risk is negligible compared to the sophisticated image or geometry editing tools that are already prevalent. Our method needs very little additional data and doesn't directly use vast internet collections with or without consent.

## Acknowledgement

We thank [Dr. Rajvi Shah](#) for her inputs in regard to bilateral search and NNFM.

## References

- [1] Benjamin Attal, Jia-Bin Huang, Michael Zollhöfer, Johannes Kopf, and Changil Kim. Learning neural light fields with ray-space embedding networks. In *Proceedings of the IEEE/CVF Conference on Computer Vision and Pattern Recognition (CVPR)*, 2022. [1](#)
- [2] Jonathan T. Barron, Ben Mildenhall, Dor Verbin, Pratul P. Srinivasan, and Peter Hedman. Mip-nerf 360: Unbounded anti-aliased neural radiance fields. In *Proceedings of the IEEE/CVF Conference on Computer Vision and Pattern Recognition (CVPR)*, pages 5470–5479, June 2022. [2](#), [3](#), [4](#), [8](#), [13](#)
- [3] Mark Boss, Raphael Braun, Varun Jampani, Jonathan T. Barron, Ce Liu, and Hendrik P.A. Lensch. Nerf: Neural reflectance decomposition from image collections. *CoRR*, 2020. [3](#)
- [4] Mark Boss, Varun Jampani, Raphael Braun, Ce Liu, Jonathan T. Barron, and Hendrik P.A. Lensch. Neural-pil: Neural pre-integrated lighting for reflectance decomposition. In *Advances in Neural Information Processing Systems (NeurIPS)*, 2021. [3](#)
- [5] Arunkumar Byravan, Jan Humplik, Leonard Hasenclever, Arthur Brussee, Francesco Nori, Tuomas Harnojo, Ben Moran, Steven Bohez, Fereshteh Sadeghi, Bojan Vujatovic, and Nicolas Heess. Nerf2real: Sim2real transfer of vision-guided bipedal motion skills using neural radiance fields, 2022. [2](#)
- [6] Mathilde Caron, Hugo Touvron, Ishan Misra, Hervé Jégou, Julien Mairal, Piotr Bojanowski, and Armand Joulin. Emerging properties in self-supervised vision transformers. *2021 IEEE/CVF International Conference on Computer Vision (ICCV)*, pages 9630–9640, 2021. [2](#), [3](#), [4](#), [11](#)
- [7] Anpei Chen, Zexiang Xu, Andreas Geiger, Jingyi Yu, and Hao Su. Tensorf: Tensorial radiance fields. In *European Conference on Computer Vision (ECCV)*, 2022. [2](#), [3](#), [4](#), [11](#)
- [8] Chong Bao and Bangbang Yang, Zeng Junyi, Bao Hujun, Zhang Yinda, Cui Zhaopeng, and Zhang Guofeng. Neumesh: Learning disentangled neural mesh-based implicit field for geometry and texture editing. In *European Conference on Computer Vision (ECCV)*, 2022. [3](#)
- [9] Akshat Dave, Yongyi Zhao, and Ashok Veeraraghavan. Pandora: Polarization-aided neural decomposition of radiance. *ArXiv*, abs/2203.13458, 2022. [1](#)
- [10] Fridovich-Keil and Yu, Matthew Tancik, Qinlong Chen, Benjamin Recht, and Angjoo Kanazawa. Plenoxels: Radiance fields without neural networks. In *CVPR*, 2022. [3](#), [4](#)
- [11] Xiao Fu, Shang-Wei Zhang, Tianrun Chen, Yichong Lu, Lanyun Zhu, Xiaowei Zhou, Andreas Geiger, and Yiyi Liao. Panoptic nerf: 3d-to-2d label transfer for panoptic urban scene segmentation. *ArXiv*, abs/2203.15224, 2022. [1](#)
- [12] Xuan Gao, Chenglai Zhong, Jun Xiang, Yang Hong, Yudong Guo, and Juyong Zhang. Reconstructing personalized semantic facial nerf models from monocular video. *ArXiv*, abs/2210.06108, 2022. [1](#)
- [13] Leon A. Gatys, Alexander S. Ecker, and Matthias Bethge. Image style transfer using convolutional neural networks. In *2016 IEEE Conference on Computer Vision and Pattern Recognition (CVPR)*, pages 2414–2423, 2016. [3](#)
- [14] Steven J. Gortler, Radek Grzeszczuk, Richard Szeliski, and Michael F. Cohen. The lumigraph. In *Proceedings of the 23rd Annual Conference on Computer Graphics and Interactive Techniques, SIGGRAPH '96*, page 43–54, New York, NY, USA, 1996. Association for Computing Machinery. [3](#)
- [15] Yudong Guo, Keyu Chen, Sen Liang, Yongjin Liu, Hujun Bao, and Juyong Zhang. Ad-nerf: Audio driven neural radiance fields for talking head synthesis. *2021 IEEE/CVF International Conference on Computer Vision (ICCV)*, pages 5764–5774, 2021. [1](#)
- [16] Kaiming He, Jian Sun, and Xiaoou Tang. Guided image filtering. *IEEE Transactions on Pattern Analysis and Machine Intelligence*, 35(6):1397–1409, 2013. [3](#)
- [17] Yi-Hua Huang, Yue He, Yu-Jie Yuan, Yu-Kun Lai, and Lin Gao. Stylizednerf: Consistent 3d scene stylization as stylized nerf via 2d-3d mutual learning. In *Computer Vision and Pattern Recognition (CVPR)*, 2022. [3](#)
- [18] Ajay Jain, Matthew Tancik, and P. Abbeel. Putting nerf on a diet: Semantically consistent few-shot view synthesis. *2021 IEEE/CVF International Conference on Computer Vision (ICCV)*, pages 5865–5874, 2021. [1](#)
- [19] Justin Johnson, Alexandre Alahi, and Li Fei-Fei. Perceptual losses for real-time style transfer and super-resolution. In Bastian Leibe, Jiri Matas, Nicu Sebe, and Max Welling, editors, *Computer Vision – ECCV 2016*, pages 694–711, Cham, 2016. Springer International Publishing. [3](#), [12](#)
- [20] Sosuke Kobayashi, Eiichi Matsumoto, and Vincent Sitzmann. Decomposing nerf for editing via feature field distillation. In *Advances in Neural Information Processing Systems*, volume 35, 2022. [2](#), [3](#), [4](#), [5](#), [6](#), [11](#)
- [21] K.N. Kutulakos and S.M. Seitz. A theory of shape by space carving. In *Proceedings of the Seventh IEEE International Conference on Computer Vision*, volume 1, pages 307–314 vol.1, 1999. [3](#)
- [22] Marc Levoy and Pat Hanrahan. Light field rendering. *Proceedings of the 23rd annual conference on Computer graphics and interactive techniques*, 1996. [3](#)
- [23] Boyi Li, Kilian Q Weinberger, Serge Belongie, Vladlen Koltun, and Rene Ranftl. Language-driven semantic segmentation. In *International Conference on Learning Representations*, 2022. [3](#), [5](#)
- [24] Feng Li, Hao Zhang, Huaizhe xu, Shilong Liu, Lei Zhang, Lionel M. Ni, and Heung-Yeung Shum. Mask dino: Towards

- a unified transformer-based framework for object detection and segmentation, 2022. [3](#)
- [25] Dominic Maggio, Marcus Abate, J. Shi, Courtney Mario, and Luca Carlone. Loc-nerf: Monte carlo localization using neural radiance fields. *ArXiv*, abs/2209.09050, 2022. [2](#)
- [26] Ricardo Martin-Brualla, Noha Radwan, Mehdi S. M. Sajjadi, Jonathan T. Barron, Alexey Dosovitskiy, and Daniel Duckworth. NeRF in the Wild: Neural Radiance Fields for Unconstrained Photo Collections. In *CVPR*, 2021. [4](#)
- [27] Lars Mescheder, Michael Oechsle, Michael Niemeyer, Sebastian Nowozin, and Andreas Geiger. Occupancy networks: Learning 3d reconstruction in function space. In *Proceedings IEEE Conf. on Computer Vision and Pattern Recognition (CVPR)*, 2019. [1](#)
- [28] Ben Mildenhall, Pratul P. Srinivasan, Rodrigo Ortiz-Cayon, Nima Khademi Kalantari, Ravi Ramamoorthi, Ren Ng, and Abhishek Kar. Local light field fusion: Practical view synthesis with prescriptive sampling guidelines. *ACM Transactions on Graphics (TOG)*, 2019. [2](#), [5](#), [12](#), [13](#)
- [29] Ben Mildenhall, Pratul P. Srinivasan, Matthew Tancik, Jonathan T. Barron, Ravi Ramamoorthi, and Ren Ng. Nerf: Representing scenes as neural radiance fields for view synthesis. In *ECCV*, 2020. [1](#), [3](#)
- [30] Thomas Müller, Alex Evans, Christoph Schied, and Alexander Keller. Instant neural graphics primitives with a multi-resolution hash encoding. *ACM Trans. Graph.*, 41(4):102:1–102:15, July 2022. [3](#)
- [31] Jacob Munkberg, Jon Hasselgren, Tianchang Shen, Jun Gao, Wenzheng Chen, Alex Evans, Thomas Mueller, and Sanja Fidler. Extracting Triangular 3D Models, Materials, and Lighting From Images. *arXiv:2111.12503*, 2021. [3](#)
- [32] Thu Nguyen-Phuoc, Feng Liu, and Lei Xiao. Snerf: Stylized neural implicit representations for 3d scenes. *ACM Trans. Graph.*, 41(4), jul 2022. [3](#)
- [33] Jeong Joon Park, Peter Florence, Julian Straub, Richard Newcombe, and Steven Lovegrove. DeepSDF: Learning continuous signed distance functions for shape representation. In *Proceedings of the IEEE/CVF Conference on Computer Vision and Pattern Recognition (CVPR)*, June 2019. [1](#)
- [34] Keunhong Park, U. Sinha, Peter Hedman, Jonathan T. Barron, Sofien Bouaziz, Dan B. Goldman, Ricardo Martin-Brualla, and Steven M. Seitz. Hypernerf: A higher-dimensional representation for topologically varying neural radiance fields. *ArXiv*, abs/2106.13228, 2021. [2](#)
- [35] Adam Paszke, Sam Gross, Francisco Massa, Adam Lerer, James Bradbury, Gregory Chanan, Trevor Killeen, Zeming Lin, Natalia Gimelshein, Luca Antiga, Alban Desmaison, Andreas Kopf, Edward Yang, Zachary DeVito, Martin Raison, Alykhan Tejani, Sasank Chilamkurthy, Benoit Steiner, Lu Fang, Junjie Bai, and Soumith Chintala. Pytorch: An imperative style, high-performance deep learning library. In H. Wallach, H. Larochelle, A. Beygelzimer, F. d'Alché-Buc, E. Fox, and R. Garnett, editors, *Advances in Neural Information Processing Systems 32*, pages 8024–8035. Curran Associates, Inc., 2019. [11](#)
- [36] Christian Reiser, Songyou Peng, Yiyi Liao, and Andreas Geiger. Kilonerf: Speeding up neural radiance fields with thousands of tiny mlps. In *2021 IEEE/CVF International Conference on Computer Vision (ICCV)*, pages 14315–14325, 2021. [3](#)
- [37] Carsten Rother, Vladimir Kolmogorov, and Andrew Blake. "grabcut": interactive foreground extraction using iterated graph cuts. *ACM SIGGRAPH 2004 Papers*, 2004. [3](#), [5](#), [13](#)
- [38] Konstantin Sofiiuk, Ilya A. Petrov, Olga Barinova, and Anton Konushin. F-brs: Rethinking backpropagating refinement for interactive segmentation. *2020 IEEE/CVF Conference on Computer Vision and Pattern Recognition (CVPR)*, pages 8620–8629, 2020. [3](#)
- [39] Pratul P. Srinivasan, Boyang Deng, Xiuming Zhang, Matthew Tancik, Ben Mildenhall, and Jonathan T. Barron. Nerv: Neural reflectance and visibility fields for relighting and view synthesis. In *arXiv*, 2020. [3](#)
- [40] Cheng Sun, Min Sun, and Hwann-Tzong Chen. Direct voxel grid optimization: Super-fast convergence for radiance fields reconstruction. In *CVPR*, 2022. [3](#), [4](#)
- [41] Cheng Sun, Min Sun, and Hwann-Tzong Chen. Improved direct voxel grid optimization for radiance fields reconstruction, 2022. [3](#), [11](#)
- [42] Matthew Tancik, Vincent Casser, Xinchun Yan, Sabeek Pradhan, Ben Mildenhall, Pratul P. Srinivasan, Jonathan T. Barron, and Henrik Kretzschmar. Block-nerf: Scalable large scene neural view synthesis. *2022 IEEE/CVF Conference on Computer Vision and Pattern Recognition (CVPR)*, pages 8238–8248, 2022. [2](#)
- [43] Ayush Tewari, Justus Thies, Ben Mildenhall, Pratul Srinivasan, Edgar Tretschk, Yifan Wang, Christoph Lassner, Vincent Sitzmann, Ricardo Martin-Brualla, Stephen Lombardi, Tomas Simon, Christian Theobalt, Matthias Niessner, Jonathan T. Barron, Gordon Wetzstein, Michael Zollhoefer, and Vladislav Golyanik. Advances in neural rendering, 2021. [3](#)
- [44] Edgar Tretschk, Ayush Tewari, Vladislav Golyanik, Michael Zollhoefer, Christoph Lassner, and Christian Theobalt. Non-rigid neural radiance fields: Reconstruction and novel view synthesis of a dynamic scene from monocular video. *2021 IEEE/CVF International Conference on Computer Vision (ICCV)*, pages 12939–12950, 2021. [2](#)
- [45] Vadim Tschernezki, Iro Laina, Diane Larlus, and Andrea Vedaldi. Neural Feature Fusion Fields: 3D distillation of self-supervised 2D image representations. In *Proceedings of the International Conference on 3D Vision (3DV)*, 2022. [2](#), [3](#), [4](#), [5](#), [6](#), [11](#), [14](#)
- [46] Wei-Cheng Tseng, Hung-Ju Liao, Yen-Chen Lin, and Min Sun. Cla-nerf: Category-level articulated neural radiance field. *2022 International Conference on Robotics and Automation (ICRA)*, pages 8454–8460, 2022. [2](#)
- [47] Richard Tucker and Noah Snavely. Single-view view synthesis with multiplane images. In *2020 IEEE/CVF Conference on Computer Vision and Pattern Recognition (CVPR)*, pages 548–557, 2020. [3](#)
- [48] Can Wang, Menglei Chai, Mingming He, Dongdong Chen, and Jing Liao. Clip-nerf: Text-and-image driven manipulation of neural radiance fields. *2022 IEEE/CVF Conference on Computer Vision and Pattern Recognition (CVPR)*, pages 3825–3834, 2022. [1](#)

- [49] Tianhao Wu, Fangcheng Zhong, Andrea Tagliasacchi, Forrester Cole, and Cengiz Oztireli. D<sup>2</sup>nerf: Self-supervised decoupling of dynamic and static objects from a monocular video, 2022. 8, 12
- [50] Yuanbo Xiangli, Linning Xu, Xingang Pan, Nanxuan Zhao, Anyi Rao, Christian Theobalt, Bo Dai, and Dahua Lin. Citynerf: Building nerf at city scale. *ArXiv*, abs/2112.05504, 2021. 2
- [51] Yiheng Xie, Towaki Takikawa, Shunsuke Saito, Or Litany, Shiqin Yan, Numair Khan, Federico Tombari, James Tompkin, Vincent Sitzmann, and Srinath Sridhar. Neural fields in visual computing and beyond. *Computer Graphics Forum*, 2022. 3
- [52] Tianhan Xu and Tatsuya Harada. Deforming radiance fields with cages. In *ECCV*, 2022. 3
- [53] Lin Yen-Chen, Peter R. Florence, Jonathan T. Barron, Tsung-Yi Lin, Alberto Rodriguez, and Phillip Isola. Nerf-supervision: Learning dense object descriptors from neural radiance fields. *2022 International Conference on Robotics and Automation (ICRA)*, pages 6496–6503, 2022. 2
- [54] Alex Yu, Ruilong Li, Matthew Tancik, Hao Li, Ren Ng, and Angjoo Kanazawa. PlenOctrees for real-time rendering of neural radiance fields. In *ICCV*, 2021. 3
- [55] Kai Zhang, Nick Kolkin, Sai Bi, Fujun Luan, Zexiang Xu, Eli Shechtman, and Noah Snavely. Arf: Artistic radiance fields, 2022. 3
- [56] Kai Zhang, Fujun Luan, Zhengqi Li, and Noah Snavely. Iron: Inverse rendering by optimizing neural sdfs and materials from photometric images. *2022 IEEE/CVF Conference on Computer Vision and Pattern Recognition (CVPR)*, pages 5555–5564, 2022. 2
- [57] Kai Zhang, Gernot Riegler, Noah Snavely, and Vladlen Koltun. Nerf++: Analyzing and improving neural radiance fields. *arXiv:2010.07492*, 2020. 4
- [58] Xiuming Zhang, Pratul P. Srinivasan, Boyang Deng, Paul Debevec, William T. Freeman, and Jonathan T. Barron. Nerf-factor: Neural factorization of shape and reflectance under an unknown illumination. *ACM Trans. Graph.*, 40(6), dec 2021. 3
- [59] Shuaifeng Zhi, Tristan Laidlow, Stefan Leutenegger, and Andrew Davison. In-place scene labelling and understanding with implicit scene representation. In *Proceedings of the International Conference on Computer Vision (ICCV)*, 2021. 3
- [60] Kun Zhou, Yaohua Hu, Stephen Lin, Baining Guo, and Heung-Yeung Shum. Precomputed shadow fields for dynamic scenes. In *ACM SIGGRAPH 2005 Papers*, SIGGRAPH ’05, page 1196–1201, New York, NY, USA, 2005. Association for Computing Machinery. 3

## Supplementary Material

### 1. Implementation Details

All the methods proposed in the paper have been implemented using PyTorch [35] branching off the code provided by DVGOv2 [41]. All experiments are performed using

a commodity hardware equipped with AMD Ryzen 5800x and a Nvidia RTX 2080Ti.

The components of the radiance fields namely the volumetric density, radiance latent vectors and the learnt DINO features are stored using VM decomposition proposed by TensoRF [7]. For radiance latent vectors, we use VM-48 representation of TensoRF is used and for DINO features, we use VM-64 variant of TensoRF. The segmentation masks have been stored as a 3D bitmap constructed as full voxel grid. Though the bitmap is having a memory in the orders of  $\mathcal{O}(n^3)$  the actual memory foot is substantially small as bitmap only requires a storage of one bit for each location in the full volumetric grid.

The DINO ViT-b8 [6] model provides 768 features for each patch of  $8 \times 8$  pixels in an image. We reduce the dimensionality of these features by doing a principal component analysis reducing the effective dimension to 64. This is consistent with the prior works [20, 45]. For each pixel, the feature is calculated by referring to the feature of the respective patch that pixel corresponds to.

We first pre-train the model for the volumetric density and radiance for 20,000 epochs. Once the radiance field is stabilized on the VM-48 TensoRF representation, we introduce distillation using *student-teacher* strategy similar to that of [20, 45] on the VM-64 TensoRF variant. Upon adoption, the resultant VM-48 variant of TensoRF along with its shallow MLP represents the radiance field, and VM-64 constitute the distilled features. It is to be noted that the distilled features are not accompanied by a shallow MLP. The features are store at voxel lattice locations and tri-linearly interpolated to be compared and optimized against the DINO features without any involvement of any non-linearity. The adoption is done with  $\lambda = 0.001$  for the weighted loss function for 5,000 epochs. The loss is taken on the features and radiance together to maintain consistency.

We choose  $K = 10$  when applying K-Means to the set of features selected from the user’s brush stroke. For the bilateral filter, the value of  $\sigma_\phi$  and  $\sigma_s$  are both set to 5.0 and the value of the threshold  $\tau$  is 0.2.

### 2. Scene Editing

In this section, we explain the procedures that were followed for editing the 3D scenes post segmentation. The segmentation procedure provides a 3D bit map representing the segmented voxels. Utilization of an additional bitmap also assists in faster rendering as the voxels with segmentation mask values of 0 can easily be filtered out. Fig. 8 shows the additional results of scene editing.

#### 2.1. Object Removal

For removing a segmented object from the scene, we alter the evaluation of the density for a 3D point. We simulta-



Figure 8. *Seamless Progressive Scene Editing*: Image (a) is the reference rendered viewpoint. In (b), the pot has been removed. Image (c) shows scene composition. The JCB from KITCHEN scene has been placed on the top of the table in the GARDEN scene. Image (d) shows appearance editing of specific objects. We apply style transfer on just the JCB. For more details please refer to Sec. 2.

neously evaluate the bit map value  $b_x$  at the queried point. To segmented the object of interest (foreground), the effective density  $\sigma'_x$  is  $\sigma_x * b_x$ . Similarly, to render the background the effective density  $\sigma'_x$  is  $\sigma_x * (1.0 - b_x)$ .

## 2.2. Translation

If an object needs to be moved to another location, the ray queries lying inside the object’s voxel space can be shifted to the desired location. Let  $t$  be the translation vector for the object to be moved, then the object’s ray-point query changes as shown below.

$$\begin{aligned} \sigma'_x, rgb'_x &= \sigma_x, rgb_x \forall b_x = 0 \\ \sigma'_x, rgb'_x &= \sigma_{x+t}, rgb_{x+t} \forall b_x = 1 \end{aligned}$$

## 2.3. Scene Composition

To perform scene composition, we follow a similar strategy used by D<sup>2</sup>NeRF [49]. We alter the volumetric rendering equation to account for density and color from both the scenes as shown below:

$$\begin{aligned} \hat{C}(r) &= \int_{t_n}^{t_f} T(t) (\sigma_1(t)c_1(t) + \sigma_2(t)c_2(t)) dt \\ T(t) &= \exp\left(-\int_{t_n}^t (\sigma_1(s) + \sigma_2(s)) ds\right) \end{aligned}$$

The results for scene composition have been shown in the main paper and Fig. 8 of the supplementary.

## 2.4. Appearance Editing

After segmentation, the object’s appearance can be altered by manipulating its  $rgb$  calculation process. In the main paper, the pot’s appearance in GARDEN scene is changed by flipping the RGB values to BGR.

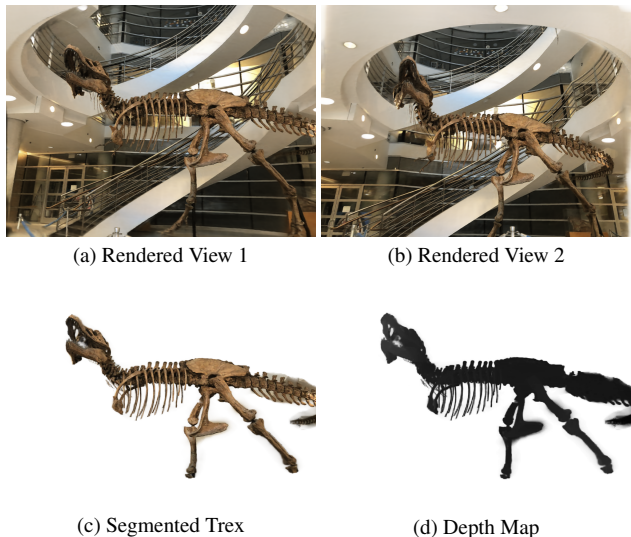


Figure 9. *Finer Segmentation*: Images (a) and (b) show rendered views of T-Rex from the LLFF dataset [28]. Image (c) shows the segmented output of T-Rex scene in LLFF dataset. We are able to achieve fine-grained segmentation of objects such as the rib-cage bones of T-Rex. However, when observed closely, the region near the tail bones contains some background as well. This is due to the background and the tail bones lying at the same distance as shown in the depth map (d). This can be mitigated by having more 3D information (better training views) or higher voxel grid resolution.

Here, we apply style transfer on an already composed scene. We first calculate a 3D bitmap for the JCB lego in the KITCHEN scene. Then, we generate a new set of stylized training images using the method proposed by [19] using a reference image. The appearance latent vectors and the rendering MLP is fine-tuned according to the new training images while keeping the density and feature weights frozen. This transfers the style from a reference image to the 3D object.

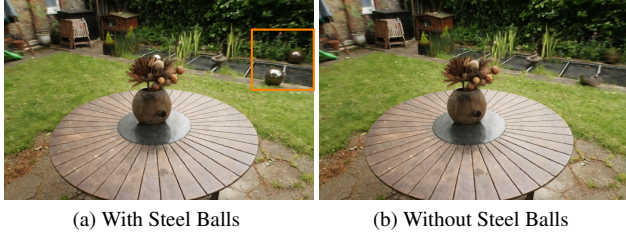


Figure 10. *Removal of Steel Balls*: We use the MipNeRF360 [2] formulation in voxel space for unbounded 360 degree scenes. This gives fewer number of voxels to the background objects compared to the central volume of interest. In this scene, we remove the steel balls appearing in the background region of the scene.

### 3. Quantitative Analysis

To quantitatively compare our method on the LLFF Dataset [28], we hand-annotate the segmentation masks for the prominent objects in the CHESS TABLE , COLOR FOUNTAIN , STOVE and SHOE RACK scenes. Tab. 1 reports the segmentation metrics for the four scenes. In our method, to predict the segmentation mask, we threshold  $\alpha$  to be greater than 0.1 while rendering. In our method, we predict the segmentation mask by filtering  $\alpha$  to be greater than 0.1 while rendering. This removes the low volumetric density seeping in that contribute negligibly in the rendered visuals.

### 4. Interactive Segmentation

Our method provides interactive segmentation capabilities to the user with the incorporation of positive and negative brush strokes similar to GrabCut [37].

Upon the addition of a new positive stroke, a new segmentation mask  $b_p$  is calculated using the procedure described in the main paper. The user has the option to grow this new region using bilateral filtering until not required. The new segmentation mask  $b_{new}$  is given by  $b \cup b_p$ .

When the user adds a negative stroke, a new segmentation mask  $b_n$  is calculated. Similar to a positive stroke, the user has the option to grow this region using bilateral filtering until not required. The new segmentation mask  $b_{new}$  is given by  $b \cap (b \cap b_n)'$  ( $X'$  denotes the complement of  $X$ ).

## 5. Critical Analysis

### 5.1. DINO Features

The teacher DINO features calculated on the training set of images are for patches of size 8x8. This method associates a total of 64 pixels to the same feature vector. As shown in Fig. 12, the teacher features appear to be in low resolution due to this. When performing the teacher-student training using the joint loss function, the features learnt by

the student are finer in detail due to assistance from volumetric density. Hence, the student surpasses the teacher during distillation. This is evident from Fig. 12 as features are allocated with distinct boundaries in the voxel space.

### 5.2. Finer Segmentation

Our method can segment out fine-grained details such as the ribs of a T-Rex as shown in Fig. 9. However, it requires accurate 3D information in order to do so. In the same T-Rex scene, the tail-bones cannot be distinguished from the wall behind since the training set images don't cover views which indicate separation between the wall and bones. Therefore, in the underlying learnt model itself, the wall and the tail bones lie at the same depth as shown in Fig. 9 (d). Additional images that cover more viewpoints can easily circumvent this issue.



Figure 11. *N3F/DFF Results*: In this figure we show result of DFF and N3F on different thresholds and in the main document we provided the best of their method. Here, we display the segmentation obtained by N3F/DFF [45]. It can be seen that despite varying the thresholds the result is poorly segmented. The background objects are starting to bleed into the foreground. For the results of our method on the same scenes, please refer to the main paper.

Scene	Metric	N3F	Ours (Patch)	Ours (Stroke)
CHESS TABLE	Mean IoU $\uparrow$	0.344	0.864	<b>0.912</b>
	Accuracy $\uparrow$	0.820	0.985	<b>0.990</b>
	mAP $\uparrow$	0.334	0.874	<b>0.916</b>
COLOR FOUNTAIN	Mean IoU $\uparrow$	0.871	<b>0.927</b>	<b>0.927</b>
	Accuracy $\uparrow$	0.979	<b>0.989</b>	<b>0.989</b>
	mAP $\uparrow$	0.871	<b>0.927</b>	<b>0.927</b>
STOVE	Mean IoU $\uparrow$	0.416	<b>0.827</b>	0.819
	Accuracy $\uparrow$	0.954	<b>0.992</b>	<b>0.992</b>
	mAP $\uparrow$	0.387	<b>0.824</b>	0.817
SHOE RACK	Mean IoU $\uparrow$	0.589	0.763	<b>0.861</b>
	Accuracy $\uparrow$	0.913	0.965	<b>0.980</b>
	mAP $\uparrow$	0.582	0.773	<b>0.869</b>

Table 1. This table denotes the Mean IoU (Intersection Over Union), Accuracy and Mean Average Precision measurements for the four LLFF scenes shown in the main paper. The ground truth segmentation masks have been hand-annotated for comparison.

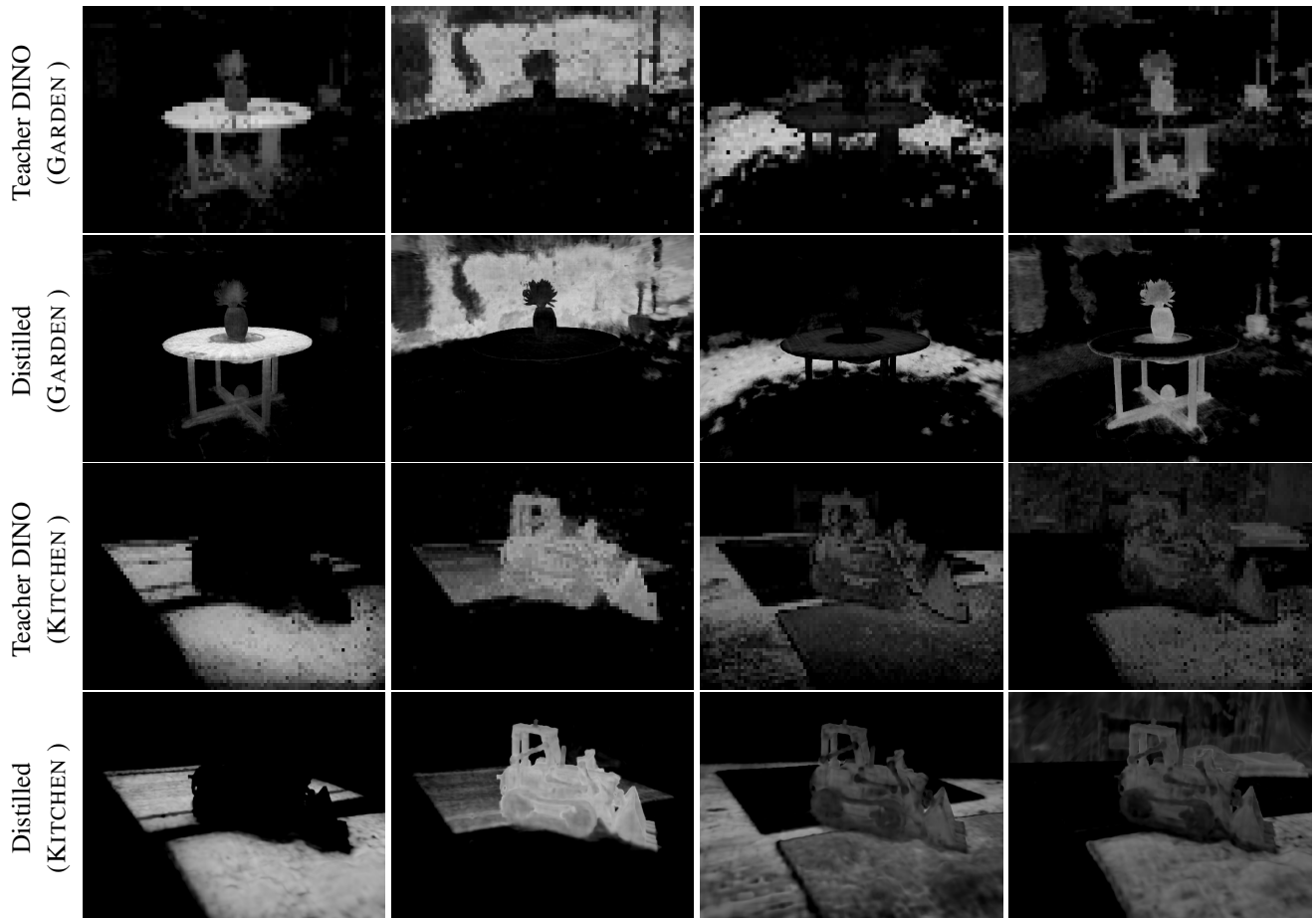


Figure 12. *Student Surpasses Teacher*: The 4 columns of this figure shows the DINO features used as teacher vs the ones learnt by student post optimization. Since, the student learns finer features than the teacher due to assistance from the volumetric density, we can claim that the student surpasses the teacher. This is consistent with the prior art N3F and DFF

Phase	Avg. Time Taken	Upper Bound
Pre-training radiance field	-	15 mins
Training feature field	-	5 mins
User stroke	3 secs	5 secs
K-Means Clustering	1.2 secs	2 secs
3D Feature Query	14 secs	20 secs
1 Iteration of Bilateral Filter	6.5 secs	10 secs

Table 2. The above table depicts the typical time taken by each phase of our method. Once the training for a given scene is done, a user can mark and get a segmented version in around 35 seconds. The user can choose to run more iterations of the bilateral filter if they wish to. The timings reported are on Nvidia's 2080Ti GPU. Note that we use python based PyTorch implementation without explicit CUDA kernels.